

34. THE GEOLOGICAL AND GEOPHYSICAL SETTING NEAR SITE 462¹

L. K. Wipperman,² Hawaii Institute of Geophysics, University of Hawaii, Honolulu, Hawaii
R. L. Larson,³ Lamont-Doherty Geological Observatory of Columbia University, Palisades, New York
and
D. M. Hussong, Hawaii Institute of Geophysics, University of Hawaii, Honolulu, Hawaii

INTRODUCTION

DSDP Site 462 is situated in the northern Nauru Basin in the western central Pacific Ocean between the eastern Caroline Islands and the Marshall Islands (Fig. 1). The primary objectives at this site were to sample Mesozoic sediments and the underlying Mesozoic oceanic crust. Previous work (Larson, 1976) has established a magnetic anomaly sequence (M16 to M25) in the central region of the Nauru Basin. South of Nauru Island, the magnetic anomalies are indistinct. North of Anomaly M25, in the northern region of the basin, the magnetic anomalies are of low amplitude, but have a distinct lineation parallel to the M16 to M25 sequence to the south (Fig. 2). Reflection profiles in the Nauru Basin show approximately 0.3 to 0.5 seconds of sediments, characterized by numerous reflectors, overlying a highly reflective "basement." Deeper reflectors are sometimes observed, however, on low-frequency reflection profile and variable-angle sonobuoy records (Houtz, 1976; Larson, 1976), suggesting that up to a kilometer of consolidated sediments or flat-lying volcanic rocks may be present beneath the upper 300 to 500 meters of unconsolidated sediments. A further seismic characteristic of the Nauru Basin, mentioned by Larson (1976) and Houtz (1976) and observed on existing unpublished HIG data, is an unusual lack of refracted arrivals observed on sonobuoy stations. Larson (1976) suggested that the lack of refractions may result from a velocity contrast across the limestone/basalt boundary which is too small to propagate refractions but large enough to produce a reflection. Houtz (1976) has suggested that the lack of refractions may be caused by alternating bands of volcanics and sediments, which would make a layer too incoherent to produce a refraction.

SITE SURVEY RESULTS

The track of the R/V *Kana Keoki* during the site selection survey of Site 462 is shown in Figure 3. The positioning was satellite-controlled. The ship's course and speed were digitally recorded every 2 seconds, and were used for dead reckoning between satellite fixes.

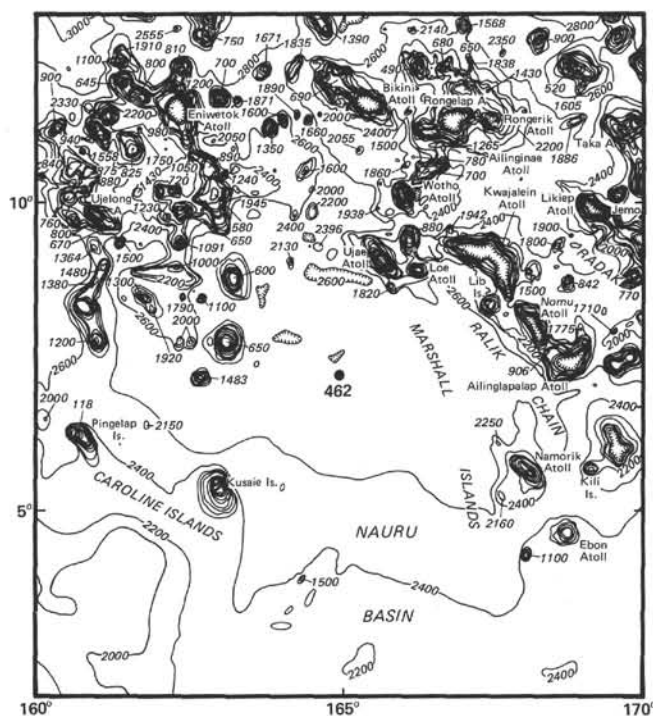


Figure 1. Regional bathymetric setting of Site 462 in the Nauru Basin, fringed to the north, east, and west by seamounts, guyots, and the Marshall and eastern Caroline islands.

Bathymetry

Figure 4 is a bathymetry contour map of the survey area. Water depth has been corrected for variations in sound velocity by using Matthew's tables. The regional depth increases from about 5100 meters in the southwest corner to 5200 meters in the northeast edge of the survey area. The bathymetry is controlled by leveed turbidity current channels which have a relief of generally less than 40 meters. The turbidity current flow is to the northeast, suggesting that the present source areas are the eastern Caroline Islands or the Ontong-Java plateau. The transition between discrete leveed channels and an extremely flat turbidite plain occurs near the center of the survey.

The 3.5-kHz and the low-frequency airgun reflection profiles indicate that the turbidity current channels producing the bathymetric relief are contained in the upper 50 to 100 meters of the sediment column. The acoustic

¹ Initial Reports of the Deep Sea Drilling Project, Volume 61.

² Present address: Mobil Exploration and Producing Services, Inc., P.O. Box 900, Dallas, Texas.

³ Present address: Graduate School of Oceanography, University of Rhode Island, Kingston, Rhode Island.

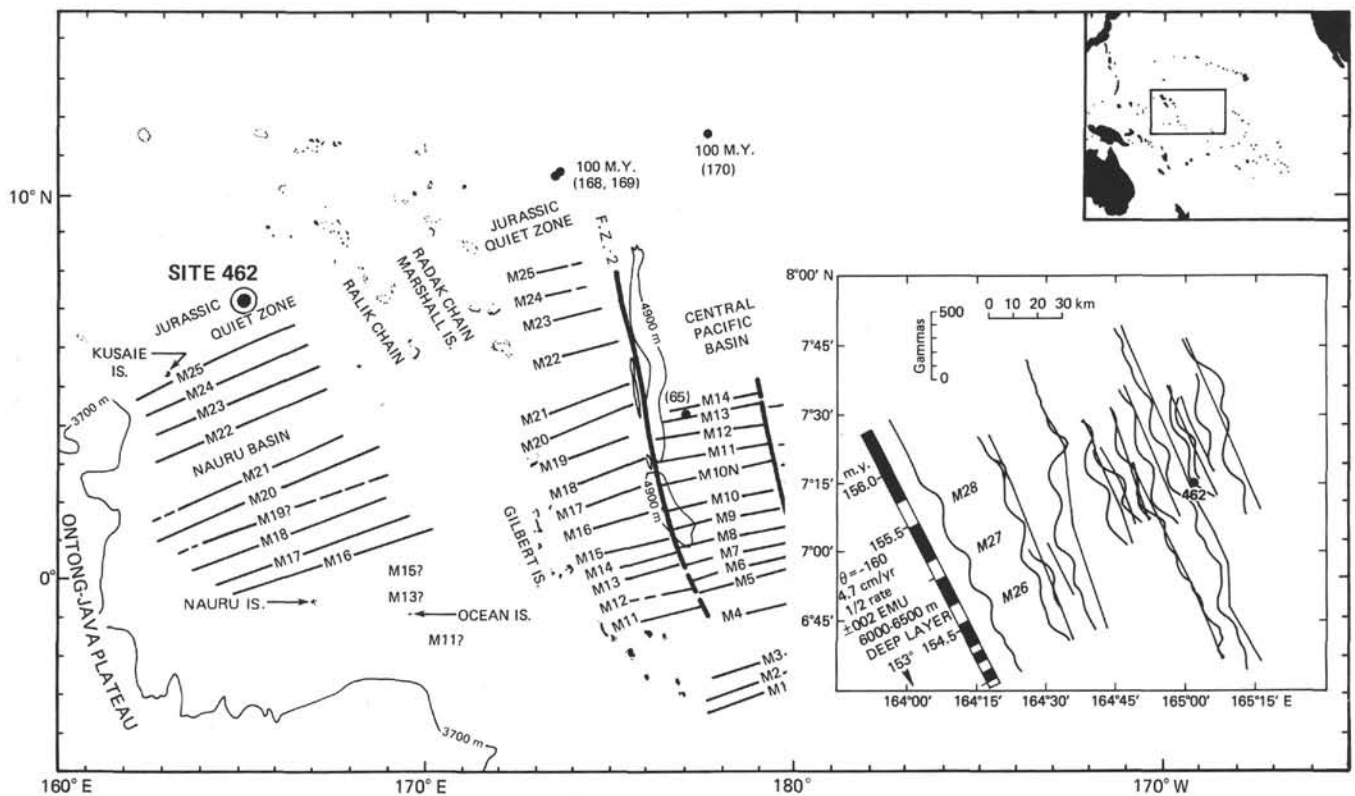


Figure 2. Mesozoic magnetic lineation patterns of the Nauru and Central Pacific basins, showing the location of Site 462 (from Larson, 1976).

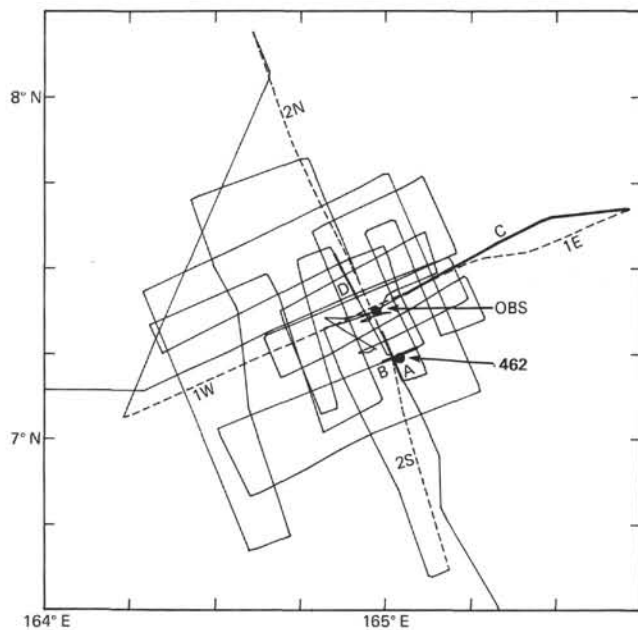


Figure 3. Chart of R/V *Kana Keoki* track during the site survey. The solid lines labeled A, B, C, and D show the locations of the reflection profiles discussed in the text. The location of the ocean-bottom seismometer is labeled OBS, and the refraction lines are dashed.

character of this interval, as seen on the 3.5-kHz profiles, falls into the following categories: (1) the turbidity current channels are highly reflective (essentially opaque); (2) the levees and surrounding high areas are acoustically transparent, with a 3.5-kHz acoustic “basement” at depths of 50 to 100 meters; and (3) alternating transparent and reflective layers exist in the remaining area. Results of piston coring and drilling at Site 462 confirm that the reflectors in this interval are fine-grained calcareous turbidites and that the transparent layers are radiolarian ooze. The shallowness of the existing turbidity current channels suggests that the locations of the channels are ephemeral.

Magnetics

Residual magnetic anomalies were calculated by removing the IGRF (1965 coefficients) from the observed total-intensity magnetic field. Magnetic profiles are plotted perpendicular to selected track lines in Figure 5. The anomaly pattern is characterized by three parallel linear anomalies with average peak-to-peak amplitude of about 80 gammas. These lineations are parallel to the M16 to M25 sequence to the south mapped by Larson (1976); Cande et al. (1979) thus considered them to be an extension of that sea-floor-spreading, magnetic-field-reversal phenomenon, and named them M26, M27, and M28. This Late Jurassic extension of the

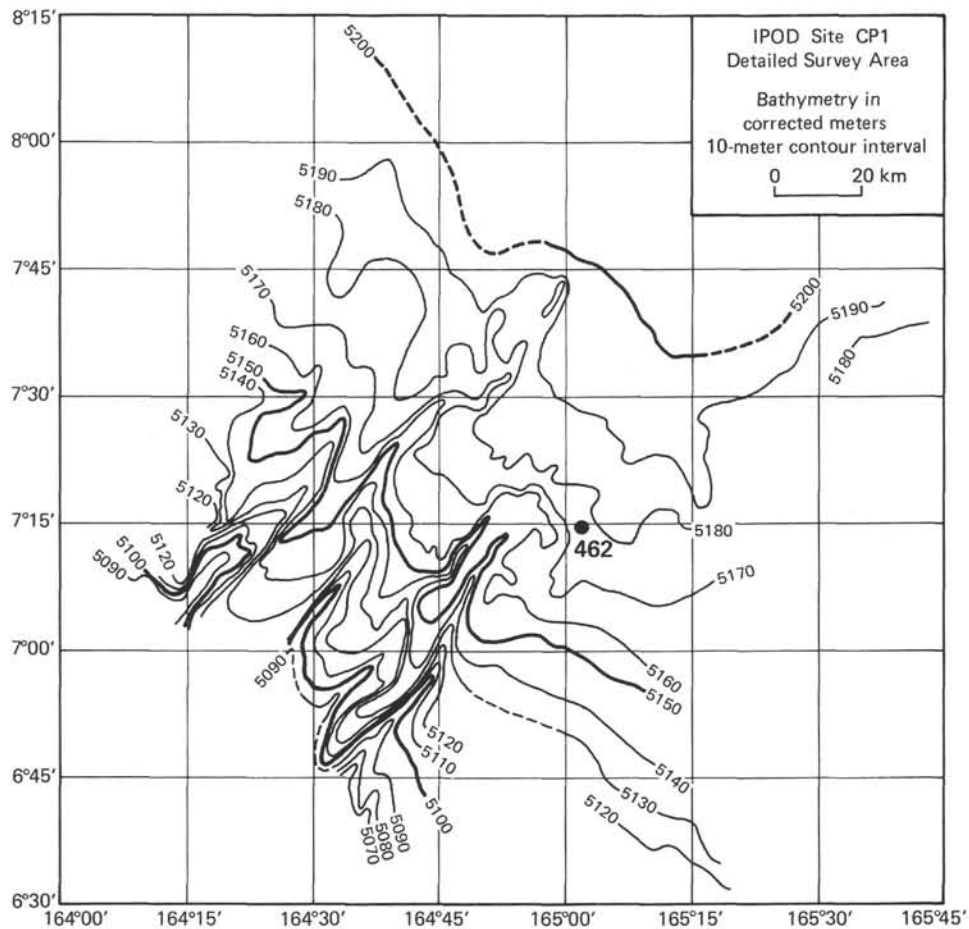


Figure 4. Bathymetry contour map. The relief consists of leveed turbidite channels.

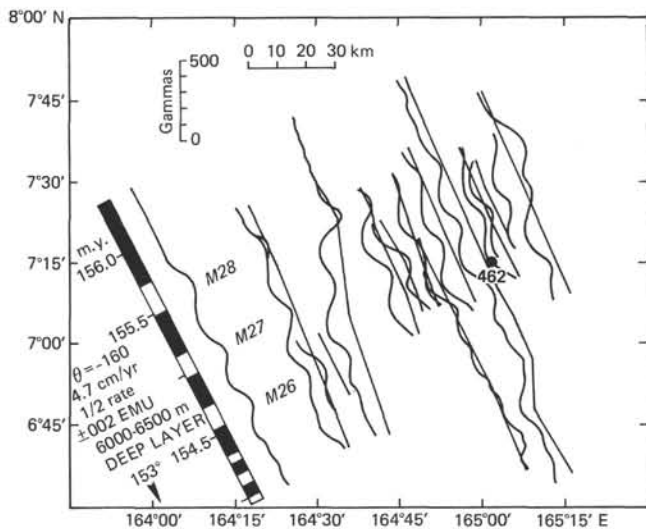


Figure 5. Cross-strike magnetic anomaly profiles across Anomalies M26, M27, and M28 in the Jurassic Quiet Zone of the northern Nauru Basin. Data are from the *Kana Keoki* site survey, and the model profile is based on the revised Late Jurassic magnetic time scale of Cande et al. (1979).

magnetic-reversal time scale was based on correlations of low-amplitude anomalies adjacent to the Phoenix, Hawaiian, and Japanese lineations, and the model for this extension is the Japanese lineations located several thousand kilometers north of the Nauru Basin. That model is shown correlated with M26, M27, and M28 in the Nauru Basin by applying a 4.7-cm/year half-spreading rate (identical to the rate used to model M21 to M25 directly to the south). Site 462 is on a normally magnetized block nominally 154.8 m.y. old. The amplitude of these anomalies is matched by a constant magnetization contrast of ± 0.002 emu, although Cande et al. (1979) modeled the entire M19 to M29 reversal sequence as a tapering amplitude envelope. They concluded that these magnetic anomalies resulted from sea-floor spreading during a 15-m.y. period when dipole magnetic field intensity increased by a factor of 4, accounting for the amplitude envelope.

Seismic Reflection

The detailed correlation of drilling results with reflection profiles is discussed by Larson and Schlanger (this volume). In the present chapter, we will discuss the stratigraphic relationships of some key horizons, deter-

mined from the interpretation of site survey reflection profiles.

Airgun reflection profiles crossing near Site 462 are shown in Figure 6 (see Fig. 3 for locations of the profiles). These sections are typical of reflection data acquired in the Nauru Basin. The reflector from the lower Eocene chert and limestone layer (labelled "Chert" in the figures) is the shallowest low-frequency reflector, and is easily correlated throughout the survey area.

The lower Eocene chert horizon is about 40 meters (about 0.03 two-way travel time) below a middle Eocene discontinuity at Site 462. The reflection profiles suggest that the thickness between the discontinuity and the

chert reflector varies a few tens of meters within the survey area. Reflection terminations appear to occur at the discontinuity rather than at the chert horizon, implying that the Eocene discontinuity is a surface of unconformity. The upper Eocene sediments onlap the Eocene unconformity, which is consistent with a substantial turbidite component of sedimentation. Reflection profile C (Fig. 7) illustrates the onlapping relationship of younger sediments onto the Eocene unconformity.

The pre-unconformity strata, which may consist primarily of the igneous complex, form the west flank of a buried "basement" high situated just east of the survey area.

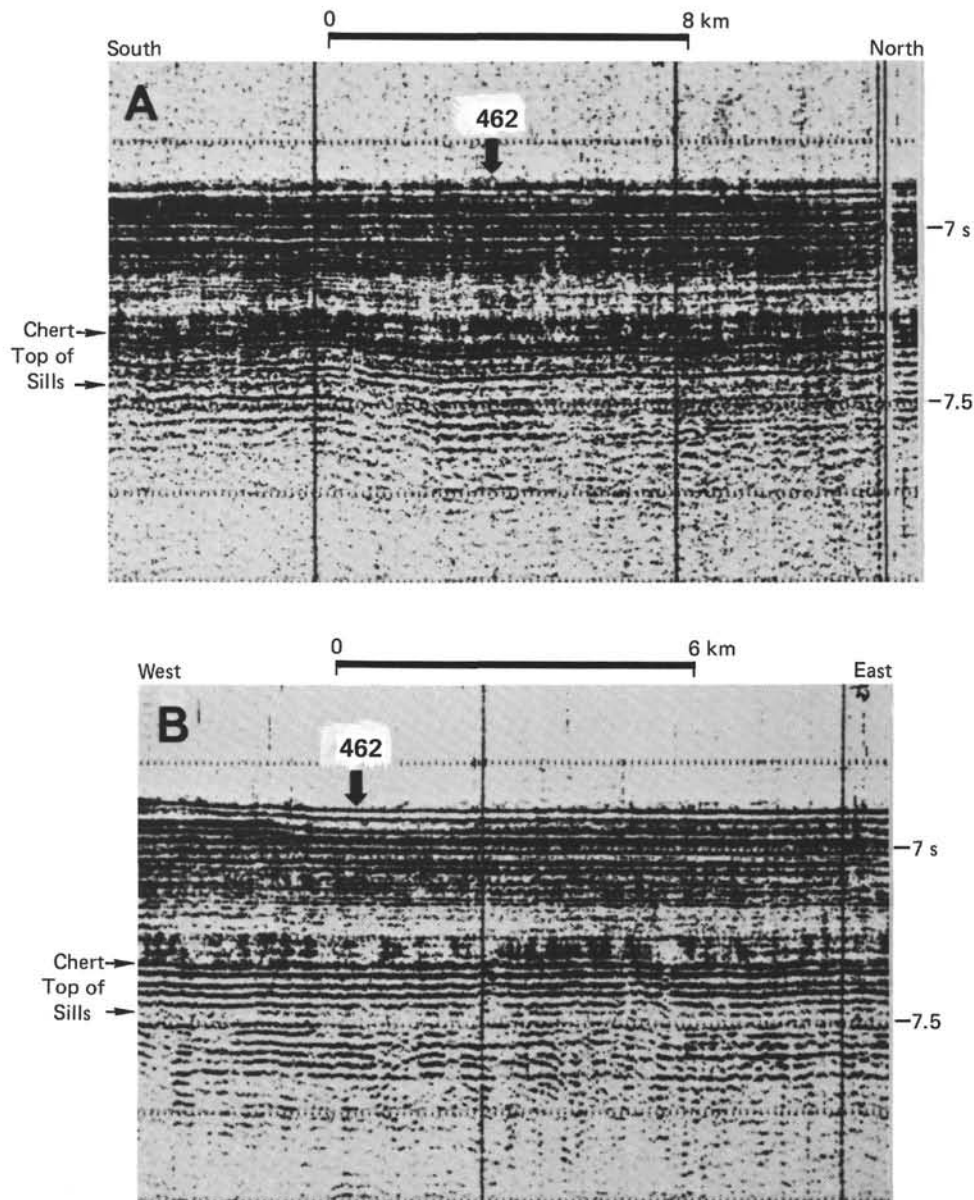


Figure 6. Reflection profiles A and B cross near Site 462. See Fig. 3 for locations. These profiles are typical of reflection data in the survey area. The reflection labeled Chert is the top of the lower Eocene chert and limestone layer. This reflection is easily correlated throughout the survey area. The reflection labelled Top of Sills is near the top of the igneous sill complex, and is difficult to observe in much of the survey area.

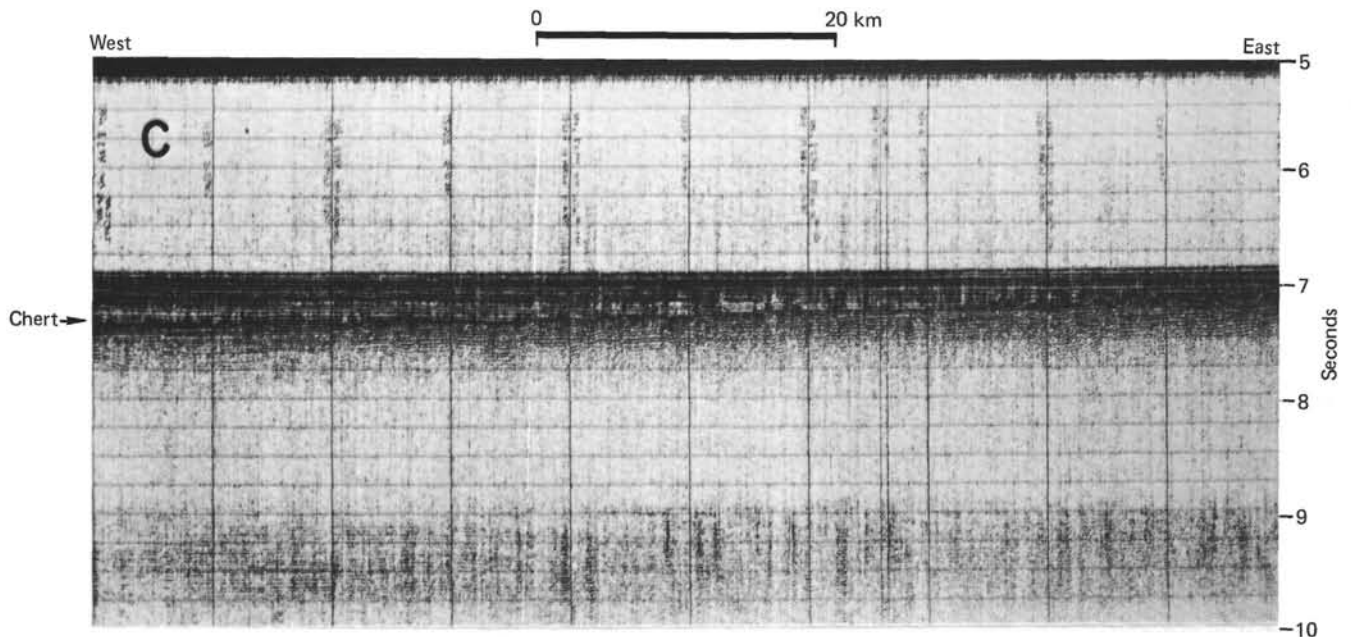


Figure 7. Reflection profile C. See Fig. 3 for location. This profile illustrates the onlap of younger sediments onto the Eocene unconformity.

The sea-floor-to-chert sediment isopach is shown in Figure 8. The chert reflector is used as the marker horizon because the Eocene unconformity is difficult to interpret over much of the survey area, where it is nearly conformable with the overlying reflectors. In addition, the chert reflector can also be used as the marker horizon for the base of the Cenozoic sediments. At Site 462, approximately 35 meters of lower Cenozoic sediment lies between the top of the lower Eocene chert and limestone layer and Upper Cretaceous sediments. The top of the Maestrichtian volcanoclastic sediments does not pro-

duce a correlatable reflector. Thus, the isopach map represents the approximate thickness of Cenozoic sediments. Reflection time between the sea floor and chert horizons was converted to thickness by using an interval velocity of 1700 m/s, determined by wide-angle reflection measurements from sonobuoys and sonic measurements at Site 462. The isopach map shows that the Cenozoic sediments generally thicken from 350 meters on the southeast edge of the survey area to about 450 meters on the northwest edge. Superimposed on the general thickness trend are variations of up to 50 meters. The western flank of the buried basement high to the east of the detailed survey is indicated by thinning Cenozoic sediments.

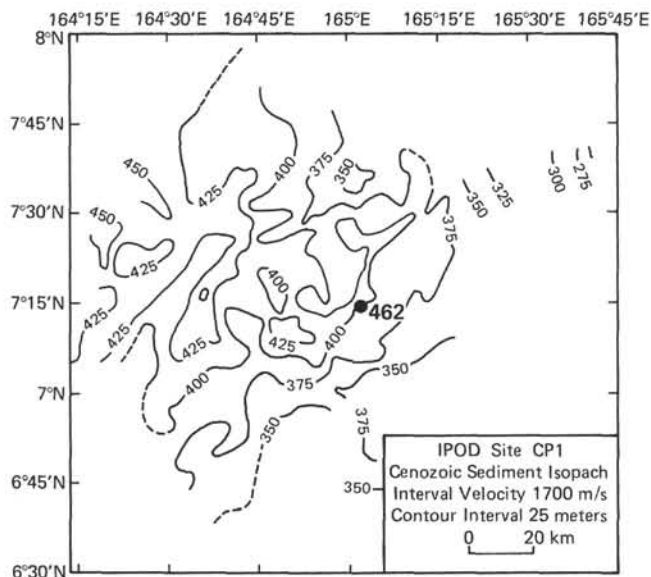


Figure 8. Sea-floor-to-chert isopach map. The isopach is the approximate thickness of Cenozoic sediments.

Depth contours on the chert reflector are shown in Figure 9. The general depth gradient is from 5450 meters at the southern edge of the survey to 5625 meters at the northern edge. The chert reflector is shallower on the western flank of the buried high to the east of the detailed survey area. Closed highs and lows, with variations of 25 to 50 meters, are superimposed on the regional depth gradient. The variations in depth to the chert horizon are correlated with the variations in thickness of the overlying sediments. Below the chert horizon, the top of the igneous complex appears as a sequence of reflectors which are generally difficult to correlate from line to line and even along the same record. When convolved with an airgun pulse, the interfingering with sediment of thin, laterally discontinuous sill units results in a complex interference pattern on reflection profiles. Profile D (Fig. 10) illustrates the changing character of the igneous complex reflection along a short segment of reflection profile. The top of the igneous complex appears as a strong reflector at a reflection time of about 7.43 s from km 0 to approximately

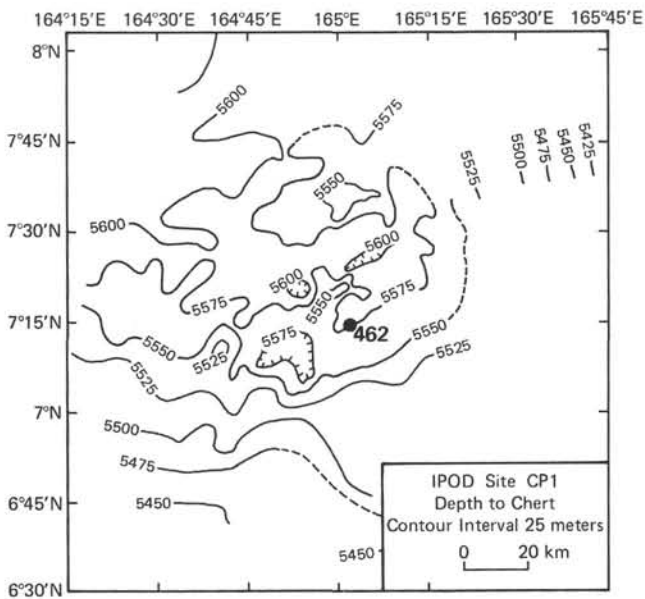


Figure 9. Map showing depth from sea level to chert. The variations in depth to the cherty horizon are correlated with variations in thickness of the overlying sediments.

km 4, changes to 7.47 s between km 4 and km 6.8, and then continues as a diffuse reflector at a time of about 7.55 s from km 6.5 to km 14. The sediment thickness between the chert horizon and the strongest reflection near the top of the igneous complex ranges from less than 20 meters to over 250 meters (0.02 to 0.23 s reflection time), but the thickness is generally about 150 to 200 meters (0.14 to 0.18 s). The interval velocity, based on

sonic measurements at Site 462, was assumed to be 2300 m/s. No regional thickness trend is apparent.

Wide-angle reflection results of seven airgun-sonobuoy measurements, made during the site survey, are summarized in Table 1. The sonobuoy profiles were devoid of refracted arrivals. Solutions were obtained for four intervals. The chert horizon produced a strong wide-angle reflection on every sonobuoy. Thus, the interval velocity and thickness from the sea floor to the chert reflector (interval 1 in Table 1) are well determined to be 1.7 km/s and 0.417 km, in good agreement with the drilling results. The interval from the chert reflector to the top of the sill complex (interval 2 in Table 1) was observed on four sonobuoys, and has an average interval velocity of 3.5 km/s and a calculated thickness of 0.452 km. Drilling results at Site 462 (see Site Summary, this volume) yielded a mean velocity and thickness for the equivalent interval of 2.5 km/s and 0.175 km. The cause of the discrepancy between the sonobuoy and drilling results is not obvious; the discrepancy may arise because of the wide-angle reflections were generated as an interference wave that was delayed with respect to the top of the sill complex, and because the thin, low-velocity, volcanoclastic sediments between the chert layer and the sill complex were not resolved. All the sonobuoy profiles detected a deeper, low-frequency reflection which occasionally has been observed on other seismic data taken in the Nauru Basin (Houtz, 1976; Larson, 1976). The weak low-frequency reflector may be present on a few of the normal-incidence reflection records acquired during the site survey, at a two-way time of 7.8 to 8.0 s. Except for the sonobuoy data, however, the arrival is too weak and intermittent to be

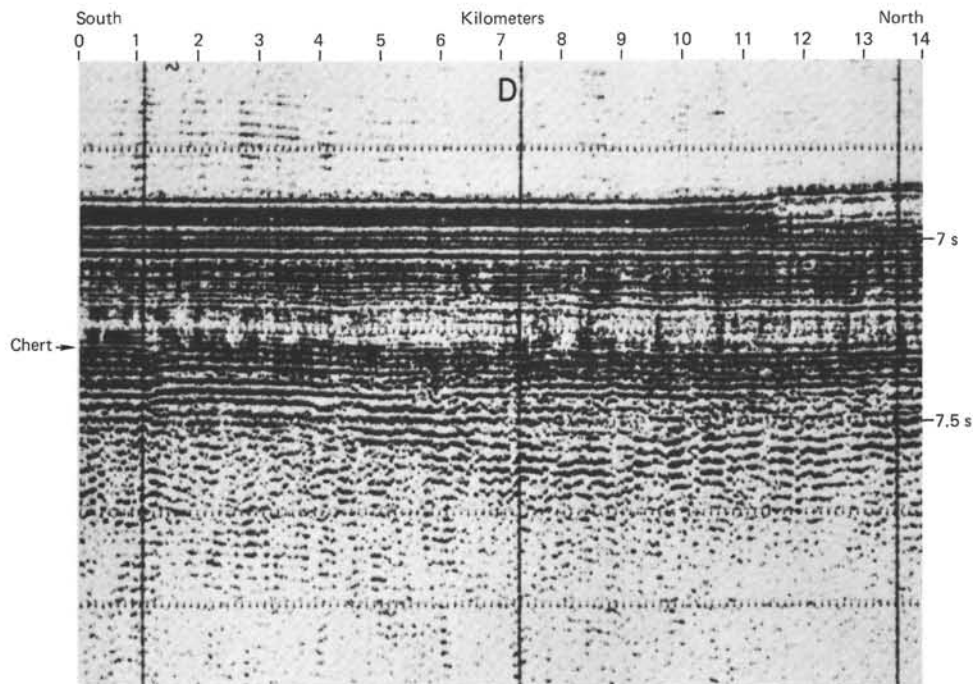


Figure 10. Reflection profile D. See Fig. 3 for location. This profile illustrates the changing character of the igneous complex reflector along a short segment of reflection profile. See text for discussion.

Table 1. Summary of sonobuoy wide-angle reflection results.

Sonobuoy No.	Receiver Position		Interval Thickness								Interval Velocity (km/s \pm S.D.)							
			Seconds				km				1		2		3		4	
	Latitude (N)	Longitude (E)	1	2	3	4	1	2	3	4	1	2	3	4	1	2	3	4
13	7°35.25	164°28.05	0.51	—	—	0.35	0.529	—	—	0.599	2.082 \pm 0.028	—	—	—	—	—	—	3.38 \pm 0.075
14	7°03.75	164°36.38	0.46	0.23	0.33	—	0.357	0.394	0.319	—	1.571 \pm 0.010	3.312 \pm 0.052	1.904 \pm 0.059	—	—	—	—	—
15	6°45.38	164°34.05	0.42	0.345	0.38	—	0.285	0.688	0.347	—	1.330 \pm 0.008	3.942 \pm 0.088	1.835 \pm 0.227	—	—	—	—	—
16	7°28.95	164°23.40	0.495	0.28	0.285	—	0.426	0.466	0.721	—	1.700 \pm 0.009	3.238 \pm 0.091	5.156 \pm 0.217	—	—	—	—	—
17	7°38.10	164°42.60	0.44	0.145	0.385	—	0.371	0.262	0.257	—	1.668 \pm 0.012	3.611 \pm 0.136	1.338 \pm 0.278	—	—	—	—	—
18	7°43.05	165°01.95	0.58	—	—	0.335	0.544	—	—	0.732	1.865 \pm 0.017	—	—	—	—	—	—	4.439 \pm 0.171
19	7°24.75	164°52.5	0.52	—	—	0.47	0.406	—	—	0.598	1.565 \pm 0.006	—	—	—	—	—	—	3.200 \pm 0.094
		Means	0.49	0.25	0.34	0.38	0.417	0.452	0.411	0.643	1.683	3.526	2.558	—	—	—	—	3.673

Note: Interval 1: Seafloor to chert reflector.
 2: Chert reflector to top of igneous complex.
 3: Top of igneous complex to deeper low-frequency reflector.
 4: Chert reflection to deeper low-frequency reflector.

meaningfully interpreted. The interval velocity and thickness for the interval between the sill reflector and the deeper reflector (3 in Table 1) are about 2.6 km/s and 0.411 km, respectively. The velocities measured in this interval may not be realistic, because the thickness of the interval is below the limit of resolution of the method. The interval velocities for interval 4 (the chert reflector to the deeper reflector) are not well determined, for the same reason.

Seismic Refraction

During the site survey, two refraction lines were shot to an array of ocean-bottom seismometers (OBS). The locations of the lines are shown in Figure 3. The lines were shot as two split profiles, crossing at the OBS array. The shot sizes ranged between 0.5 kg near the OBS and 54 kg at the maximum range of 80 to 90 km.

The OBS data were originally recorded on analog cassette tape on four channels: hydrophone with minute mark, vertical geophone, horizontal geophone, and time code. The data were digitized and then processed and displayed on the HIG Harris computer system.

Velocity-depth functions were determined by several methods. First, straight-line segments were visually fit to the first arrivals, and velocity-depth models consisting of constant-velocity layers with first-order discontinuities were calculated by the slope-intercept method. The slope-intercept models are summarized in Table 2. The velocities and thicknesses of the 1.7- and 3.5-km/s layers are from the sonobuoy wide-angle reflection results, because no refracted arrivals from the shallow layers were observed. The slope-intercept velocity models indicate a thicker than normal Layer 2, a depth to moho of about 14 km, and an upper mantle velocity which is slightly greater in a direction perpendicular to the magnetic anomalies. In order to better constrain the possible velocity-depth functions by using arrival amplitude distribution, in addition to the travel times, synthetic seismograms were calculated by the reflectivity method and visually compared with the observed record sections. The candidate velocity-depth functions were adjusted until a good match was obtained between the synthetic and observed seismograms.

The data on three of the refraction lines (1E, 1W, and 2N) require a low-velocity zone (LVZ) in the upper

Table 2. Slope-intercept velocity-depth functions.

Line 1E		Line 1W	
Depth (km)	Velocity (km/s)	Depth (km)	Velocity (km/s)
0.0	1.51	0.0	1.51
5.19	1.7	5.19	1.7
5.59	3.5	5.59	3.5
6.00	5.36	5.93	5.37
7.39	5.55	7.57	5.53
8.79	6.42	9.91	7.17
11.84	7.51	12.14	7.53
		14.60	8.04
Line 2N		Line 2S	
0.0	1.51	0.0	1.51
5.19	1.7	5.19	1.7
5.59	3.5	5.59	3.5
5.87	4.97	6.18	5.01
8.43	6.27	6.64	5.39
11.07	7.42	8.59	6.53
13.48	8.22	10.92	7.31

crust. Refraction lines 2S does not require an LVZ to match the amplitude and travel-time data. Synthetic seismogram analysis also showed that most of the velocity changes in the crust were gradational.

Figure 11 shows a comparison of the velocity-depth functions for the upper 4000 meters of the crust, derived from the site survey seismic data and the velocity-depth function measured by the sonic log and determined on samples recovered from Site 462. Except for the LVZ on the 1W velocity-depth function, the two refraction curves have similar velocities. This suggests that, even though it does not exhibit the characteristics of an LVZ, the velocity function of the upper crust in the region of line 2S is similar to those at the other refraction lines. It is apparent from Figure 11 that the average velocity-depth function determined by the wide-angle reflection measurements predicted very well the depth to the lower Eocene chert horizon. The depth to the igneous complex was not as well determined, however. This wide-angle reflection method placed the top of the igneous complex at 700 meters sub-bottom, although the predicted depth was changed to about 950 meters with the addition of the refraction data.

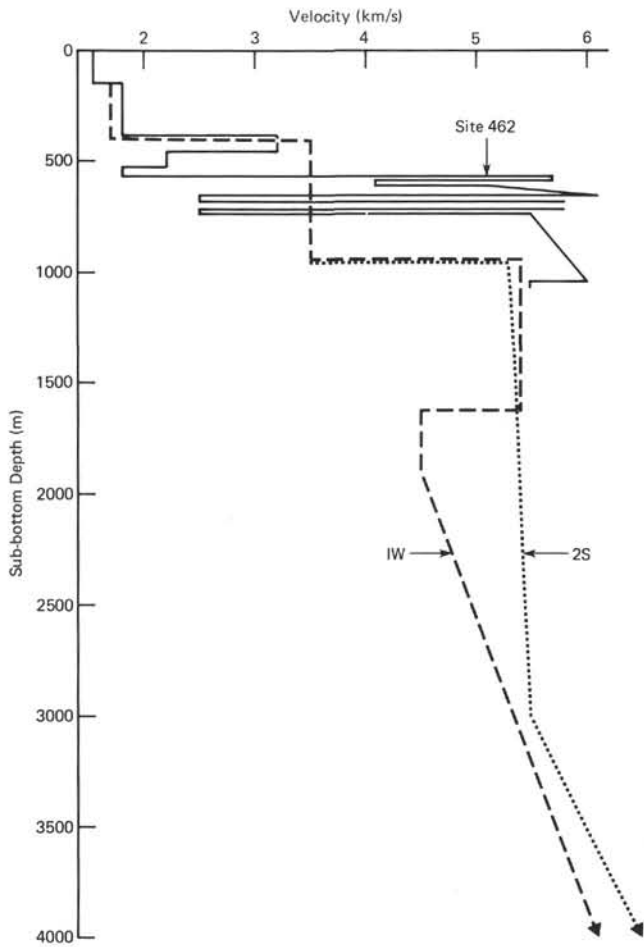


Figure 11. A comparison of the velocity–depth functions derived from site survey seismic data (1W and 2S) and the velocity–depth function measured by the sonic log and determined on recovered samples from Site 462.

CONCLUSIONS

The results of the site survey preceding the drilling at Site 462 not only provided a detailed data base from which to choose a safe and appropriate drilling location, but also shed light on several scientific problems. The magnetic data demonstrated that at least three linear magnetic anomalies occur in the Jurassic Quiet Zone and are parallel with the previously known Mesozoic anomalies. The OBS refraction data generally require the presence of a low-velocity zone in the upper crust. The cause of the velocity inversion in the upper crust is not known. However, three possibilities are that (1) the top of the older ocean crust has a lower velocity than the rocks of the overlying igneous sill complex; (2) several hundred meters of Lower Cretaceous and Upper Jurassic sediments lie between the middle Cretaceous igneous complex and the Jurassic ocean crust; and (3) the LVZ is not directly related to the presence of the igneous complex, but results from lithology or chemical alteration within the crust. The third possibility has, perhaps, the most significance, because the conditions causing the velocity inversion could be expected to be more common than the first two.

REFERENCES

- Cande, S. C., Larson, R. L., and LaBrecque, J. L., 1979. Magnetic lineations in the Pacific Jurassic quiet zone. *Earth Planet. Sci. Lett.*, 41:434–440.
- Houtz, R. E., 1976. Seismic properties of Layer 2A in the Pacific. *J. Geophys. Res.*, 81:6321–6331.
- Larson, R. L., 1976. Late Jurassic and Early Cretaceous evolution of the western Central Pacific Ocean. *J. Geomag. Geoelectr.*, 28:219–236.